RGNZ/MGPB

Toward a GIC Hazard Model for Indonesia: Analysing Latitudinal Effects of Geomagnetic Storms on the 210° Magnetic Meridian

Rudarsko-geološko-naftni zbornik
(The Mining-Geology-Petroleum Engineering Bulletin)
DOI: 10.17794/rgn.2026.5.10

Original scientific paper

Setyanto Cahyo Pranoto[1], Anwar Santoso[1,2]*, Sismanto Sismanto[2], Eddy Hartantyo[2], Rhorom Priyatikanto[1], Nizam Ahmad[3], Silmie Vidiya Fani[1], Djohar Syamsi[3], Kuncoro Wisnu[1], Mario Batubara[1], Fitri Nuraeni[1], Siska Filawati[1], Muzirwan[4]

[1] *Research Center for Space, National Research and Innovation Agency, Bandung 40173, Indonesia.*
[2] *Physics Department, Faculty of Mathematics and Natural Sciences, Gadjah Mada University, Yogyakarta, Indonesia.*
[3] *Research Center for Smart Mechatronics. National Research and Innovation Agency, Bandung, Indonesia.*
[4] *Research Center for Climate and Atmospheric, National Research and Innovation Agency, Jakarta, Indonesia.*

Abstract

Geomagnetically induced currents (GICs) arise during geomagnetic storms, which alters ionospheric and magnetospheric current systems from auroral to equatorial latitudes. This study examines the latitudinal response of the H-component (ΔH) during 91 storm events (56 coronal mass ejection (CME)-driven and 35 corotating interaction regions (CIR)-driven) from 1992 to 1999. This study uses data from 29 observatories along the 210° magnetic meridian (MM), both storm types exhibit a distinct inverted-omega (ω) latitudinal structure, the biggest around the aurora, characterized by a strong auroral electrojet (AE), minima near ~±50° magnetic latitude, and enhanced low-latitude disturbances linked to equatorial electrojet (EEJ) currents. CME-driven storms produce larger ΔH amplitudes and steeper gradients due to impulsive forcing and prompt penetration electric fields (PPEFs), whereas CIR-driven storms show weaker but more persistent responses influenced by disturbance dynamo electric fields (DDEFs) processes. In the Indonesian sector, at Biak and Pontianak (~9°–17° S magnetic latitude), low-latitude responses are comparable to near-equatorial observations, indicating efficient penetration of equatorial electrodynamics. Despite smaller absolute ΔH amplitudes than at auroral latitudes, these responses remain spatially coherent and significant. The transition region near ~±50° magnetic latitude and the distinct day-night asymmetry between storm types provide important constraints for GIC hazard assessment in equatorial power systems. Usually, the large ΔH in CME-driven storms is often accompanied by an enhanced dB/dt. The geomagnetic storms by CME-driven can generate significant geoelectric fields even at low latitudes. The results show that Indonesia is not immune to the hazards associated with GIC. The observed systematic structure (ω) and associated geoelectric fields provide new evidence that Indonesia's regions are potentially subject to substantial GIC impacts, particularly with CME-driven storms.

Keywords:
geomagnetic storm; equatorial electrojet (EEJ); coronal mass ejection (CME); corotating interaction region (CIR); 210° magnetic meridian

1. Introduction

The near-Earth's space environment is strongly influenced by solar activities, such as Coronal Mass Ejections (CMEs) and Corotating Interaction Regions (CIRs). CIRs are generated by Coronal Hole (CH) phenomena. During CME or CIR events, energetic particles and magnetic fields are spread in all directions carried away by the solar wind. The interaction between the solar wind and the southward component of the Interplanetary Magnetic Field (IMF Bz) produces geomagnetic storms that affect global current systems within the magnetosphere-ionosphere coupling, including human technological infrastructure (**Kamide et al., 1998; Borovsky & Denton, 2006; Burns et al., 2012; Chi et al., 2016; Hajra & Sunny, 2022; Ahmad et al., 2018, 2025**). Based on their driving mechanisms, geomagnetic storms are broadly categorized into CME-driven storms and CIR-driven storms. CME-driven storms are typically stronger and short-lived, often preceded by a Sudden Storm Commencement (SSC) and a significant southward component of the Interplanetary Magnetic Field (IMF Bz). In contrast, CIR-driven storms tend to be moderate, long-lasting, and recurrent, especially during the declining phase of the solar cycle (**Cane & Rich-**

* Corresponding author: Anwar Santoso
e-mail address: anwa011@brin.go.id
Received: 2 February 2026. Accepted: 11 May 2026.
Available online: 26 October 2026

ardson, 2003; Turner et al., 2006; Shen et al., 2017, Santoso et al., 2025a).

The input of energy into the magnetosphere during storms enhances the large-scale in the ionospheric current systems. At high latitudes, intensification of the auroral electrojet (AE) reflects stronger magnetosphere-ionosphere coupling and enhanced plasma convection. Meanwhile, at low latitudes, penetration of magnetospheric convection electric fields and storm-time dynamo processes modulate the equatorial electrojet (EEJ), causing changes in the horizontal geomagnetic field near the magnetic equator (**Kikuchi & Hashimoto, 2016; Yamazaki & Maute, 2017; Fejer et al., 2008**). Overall, current systems across different latitudes collectively determine the spatial and temporal characteristics of geomagnetic disturbances during storms.

Rapid variations in the geomagnetic field at the Earth's surface (*dB/dt*) can generate Geomagnetically Induced Currents (GICs) in grounded technologies, such as power transmission networks, underground pipelines, and telecommunication systems (**Boteler et al., 1998; Pulkkinen et al., 2012; Love & Swidinsky, 2014**). Although GICs are typically largest at auroral and subauroral latitudes during strong geomagnetic storms, several recent studies have reported measurable GICs at mid- and low latitudes, including in Australia, Brazil, China, Japan, and Malaysia (**Liu et al., 2009; Marshall et al., 2013; Barbosa et al., 2015; Watari et al., 2021; Khurshid et al., 2022**). These findings indicate that low-latitude regions are also potentially vulnerable to transformer saturation, reactive power loss, and cumulative thermal degradation caused by recurrent storm-time currents (**Zawawi et al., 2020**), thus motivating further GIC study in Indonesia.

Indonesia is located near the magnetic equator and is traversed by the 210° Magnetic Meridian (210° MM), a coordinated multi-latitude geomagnetic observation network extending from high latitudes to the equator (**Yumoto et al., 1996**). This longitudinal sector provides an important opportunity to investigate latitude-dependent storm responses within a unified meridian framework. Although the 210° MM network has been operating for several decades, the complete characteristics of horizontal geomagnetic disturbances (ΔH) along the meridian, particularly the transition between AE influences at high latitudes and EEJ effects near the magnetic equator, remain insufficiently quantified. Most previous studies have focused on high- and mid-latitude responses, leaving uncertainties regarding the magnitude, spatial structure, and local-time dependence of responses at low latitudes that are useful for further study concerned with the potential of GIC generation and the probability of hazardous effects at low-latitudes, particularly in Indonesian areas (**Uozumi et al., 2008; Ngwira et al., 2013; Pulkkinen et al., 2017; Tozzi et al., 2019**).

This study aims to address these gaps by evaluating the potential for GICs in Indonesia and their possible impacts on the Indonesian power grid. The analysis uses variations in the horizontal geomagnetic field component (*dH/dt*) from 29 stations along the 210° MM (-65° to +70° magnetic latitude) during 91 geomagnetic storms (Dst ≤ -50 nT) between 1992 and 1999. This parameter is essential for GIC formation (**Kataoka & Ngwira, 2016; Kasran et al., 2018; Dimmock et al., 2020; Santoso et al., 2025b**). By classifying storms according to their drivers (CME or CIR) and local-time sectors (day or night), the study quantifies the latitudinal morphology of ΔH responses and identifies the transition latitude between auroral and equatorial current systems. Additionally, disturbance amplitudes observed at the two Indonesian stations (Biak and Pontianak) are assessed to evaluate their potential contribution to GIC exposure at low latitudes and also their potential impact.

2. Data And Methods

2.1. Geomagnetic Data

This study uses measurements of the horizontal magnetic field component (H-geomagnetic field) from 29 ground-based geomagnetic stations located along the 210° MM between -65° and +70° magnetic latitude (MLAT) (see **Figure 1**). This network established and lead by the Space Environment Research Center of Kyushu University (**Yumoto et al., 1996**), provides a unique multi-latitude dataset for analysing geomagnetic storm responses under nearly constant magnetic local time (MLT) conditions. Two stations are located in Indonesia, at Pontianak (-16.96° MLAT) and Biak (-9.74° MLAT). All magnetic field data were converted into hourly averages in the HDZ coordinate system to maintain consistent temporal resolution. Quiet-day baselines were determined for each station using the standard quiet-day list provided by the World Data Center for Geomagnetism, Kyoto.

Geomagnetic storms analyzed in this study were selected from the period 1992–1999, covering the end of the declining phase of Solar Cycle 22 and the early rising phase of Solar Cycle 23. Storm intervals were identified using the criterion of moderate to strong geomagnetic storm with a Dst minimum ≤ -50 nT with a total of 91 identified storm events. This study focuses on diurnal geomagnetic storm-time (day-night). The observed morphology is expected to be predominantly governed only by dayside and nightside storms. Each event was subsequently classified according to its solar wind driver (CME and CIR-driven storms) and the magnetic local time of occurrence. Storm drivers were determined using published CME and CIR storm catalogues (**Cane & Richardson, 2003; Turner et al., 2006; Chi et al., 2016; Shen et al., 2017; Pandya et al., 2019; Hajra & Sunny, 2022; Santoso et al., 2025a**), supplemented with manual classification based on OMNI solar wind parameters (https://omniweb.gsfc.nasa.gov/form/dx1.html) for events not included in the catalogues. The list of geomagnetic storm events, including CME-driven storms

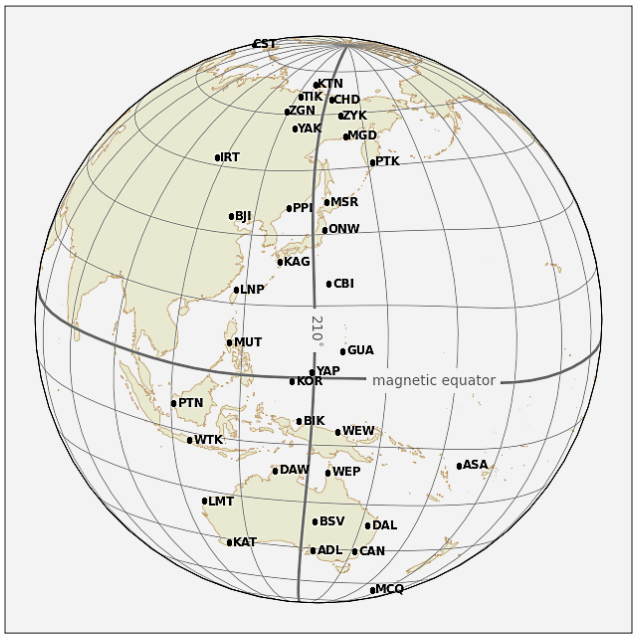


Figure 1: The 210° MM network locations. The two geomagnetic observatories located in Indonesia, namely the PTN at Pontianak and BIK at Biak, both of which provide data for the period considered in this study. The list of geomagnetic observatories is shown in **Table A1** (**Supplementary data**).

and CIR-driven storms, are presented in **Tables A2.a** and **A2.b** (**Supplementary data**). The classification of daytime and nighttime conditions (local time) refers to **Clúa de Gonzalez and Gonzalez (2013)**.

2.2. Storm Driver Identification

Several indices can be used to measure the intensity of geomagnetic storms. In this study, we analyzed hourly mean values of the horizontal magnetic field (in the HDZ system) and calculated the disturbance amplitude ΔH, defined as the difference between the observed horizontal magnetic field and the quiet-day baseline:

$$\Delta H(t) = H(t) - H_{sq}(t) \quad (1)$$

where *DH(t)* is the local disturbance of *H*-geomagnetic field component at the time of t, *H(t)* is the observed *H*-geomagnetic field component at time of t, the quiet-day reference field, H_{sq} is the average of *H*-geomagnetic field component of the five quietest days within a given month follows **Santoso et al. (2025b)**, building upon the formulation of **Yamazaki and Maute (2017)**, which is ultimately rooted in the classical work of **Chapman and Bartels (1940)**.

$$H_{sq} = \frac{1}{5}\sum_{q=1}^{5} H_q \quad (2)$$

For each storm and station, the minimum disturbance value of ΔH (ΔH_{min}) was extracted at the time of the geomagnetic storm. This event-centered metric represents the peak electrodynamics forcing state of each storm and provides a physically relevant measure of maximum geomagnetic disturbance, which is particularly pertinent to studies of geomagnetically induced currents (GICs).

2.3. Latitudinal Normalization and Local Time

The latitudinal structure of storm-time geomagnetic disturbances along the 210° MM was analyzed by compiling ΔH_{min} values from all stations for each storm. Latitudinal profiles for each driver class (CME and CIR) were generated by mapping and averaging observatory data as a function of magnetic latitude to describe their distinct spatial responses. Moreover, to extract large-scale morphological features, such as equatorial plateaus, auroral enhancements, and transition regions between current systems, a fifth-order polynomial was applied as a morphological smoothing operator rather than a statistical best-fit model. This approach emphasizes the characteristic inverted-omega (ω) latitudinal structure while suppressing small-scale station-to-station variability. The polynomial is applied due to the observed morphology of the data distribution, characterized by maximum responses at high latitudes and a quasi-exponential decrease toward lower latitudes. Sensitivity test analysis using various orders of polynomial demonstrates that the fifth-order polynomial provides the best fit to the latitudinal morphology of geomagnetic field responses during geomagnetic storms.

All latitudinal profiles were normalized to the Biak station, which serves as a representative low-latitude reference. This normalization enables direct comparison of storm amplitudes across latitudes and supports assessment of how geomagnetic disturbances in Indonesia compare with higher-latitude regions where GIC impacts are traditionally more significant.

Furthermore, we examined the geomagnetic disturbances separately for daytime and nighttime conditions since solar illumination and ionospheric conductivity have a significant impact on storm electrodynamics. Local time was established using the magnetic meridian reference longitude (UT + 9 hours), ensuring consistency across stations and alignment with the Biak sector. A storm was classified as a daytime event if the minimum Dst occurred between 06:00 and 18:00 LT while if it occurred between 18:00 and 06:00 LT defined as a nighttime. This separation allows examination of how solar controlled ionospheric processes, such as enhanced Cowling conductivity and penetrating convection electric fields during daytime or westward electrojet activity during nighttime, affect storm-time ΔH responses. Using this classification, 56 CME-driven storms (38 daytime and 18 nighttime) and 35 CIR-driven storms (18 daytime and 17 nighttime) were identified (see **Appendix Tables 2a** and **2b**). This dataset provides a robust and consistent basis for assessing how solar wind drivers and local time influence the latitudinal geomagnetic response along the 210° MM.

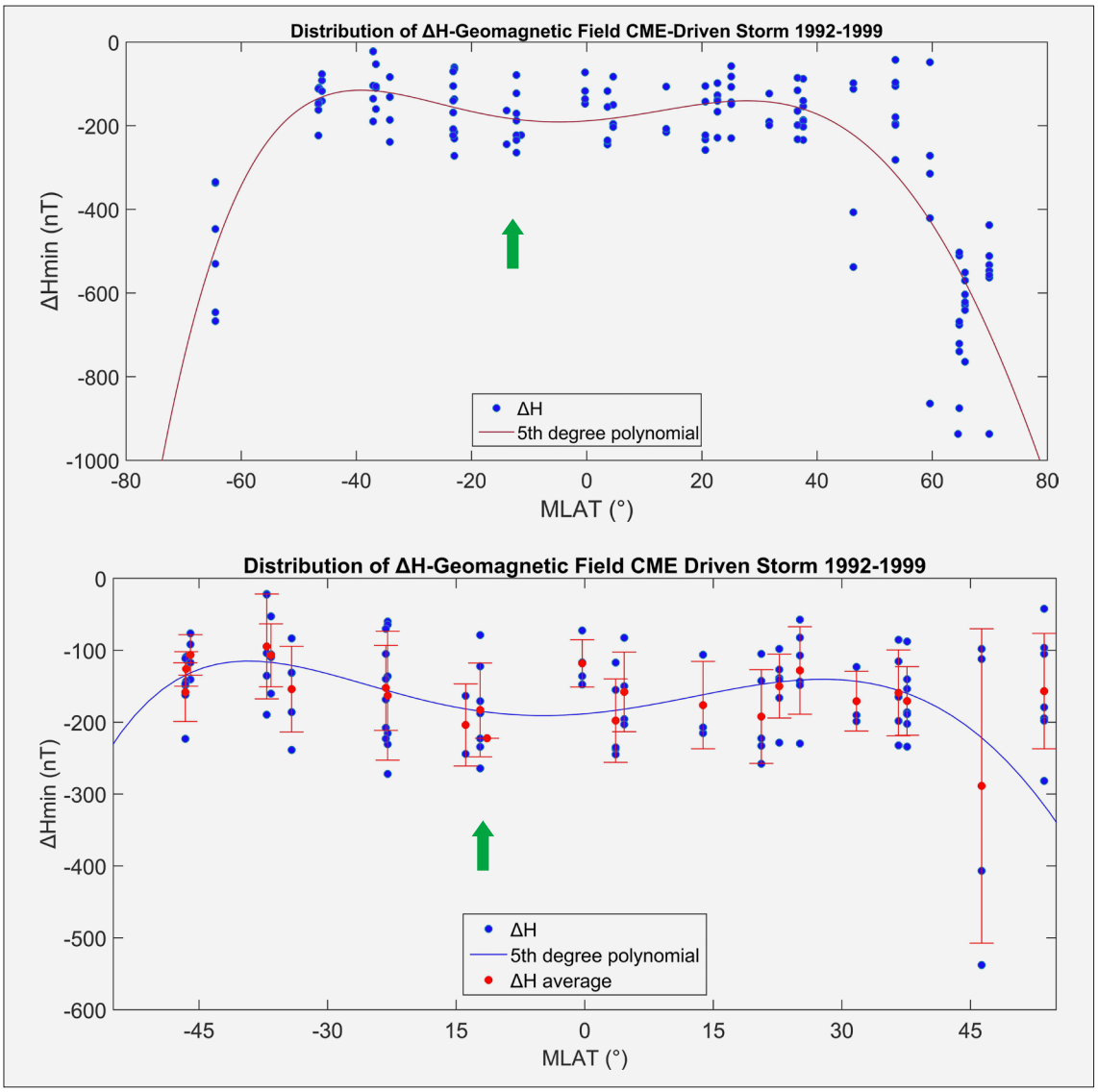


Figure 2: Latitudinal profile of DH_{min} during CME-driven storms between 80°N and 80°S (top) and Average DH_{min} during CME-driven storms between 55°S and 55°N (bottom). The green arrows indicate the locations of the Biak and Pontianak observatories.

This study systematically assesses the characteristic of day and night differences linked to each interplanetary driver and their impact on the latitudinal morphology of geomagnetic disturbances along the 210° magnetic meridian by applying local-time classification to both CME- and CIR-driven storms.

3. Results

We first examined the ΔH_{min} related to CME and CIR. **Figures 2** and **3** present the latitudinal profile of ΔH_{min} during CME- and CIR-driven storms along the 210° magnetic meridian (MM), with geomagnetic latitudes of approximately ±80° and ±55° for the period 1992-1999.

The latitudinal distribution of ΔH_{min} during CME-driven geomagnetic storms from 1992 to 1999 throughout a broad range of magnetic latitudes (MLAT) is shown in the top panel of **Figure 2**. Strong ionospheric and magnetospheric current increases at these latitudes are identified by a sharp decline in ΔH_{min} toward extremely negative values. Low and mid-latitudes, on the other hand, have very mild ΔH_{min} values that are grouped between roughly -100 and -300 nT. With a large maximum (less negative ΔH_{min}) at equatorial and mid-latitude regions, the fitted fifth-degree polynomial clearly shows a latitudinal dependence. The top panel of **Figure 2** shows that polynomial pattern indicates relative geomagnetic stability close to the magnetic equator during CME-driven storms. There is also a discernible imbalance between high latitudes in the north and south, suggesting potential hemispheric variations in storm-time current systems. The dominance of auroral electrojets is reflected in the polynomial curve's abrupt drop at high MLAT. Overall, the graphic shows that the effects of

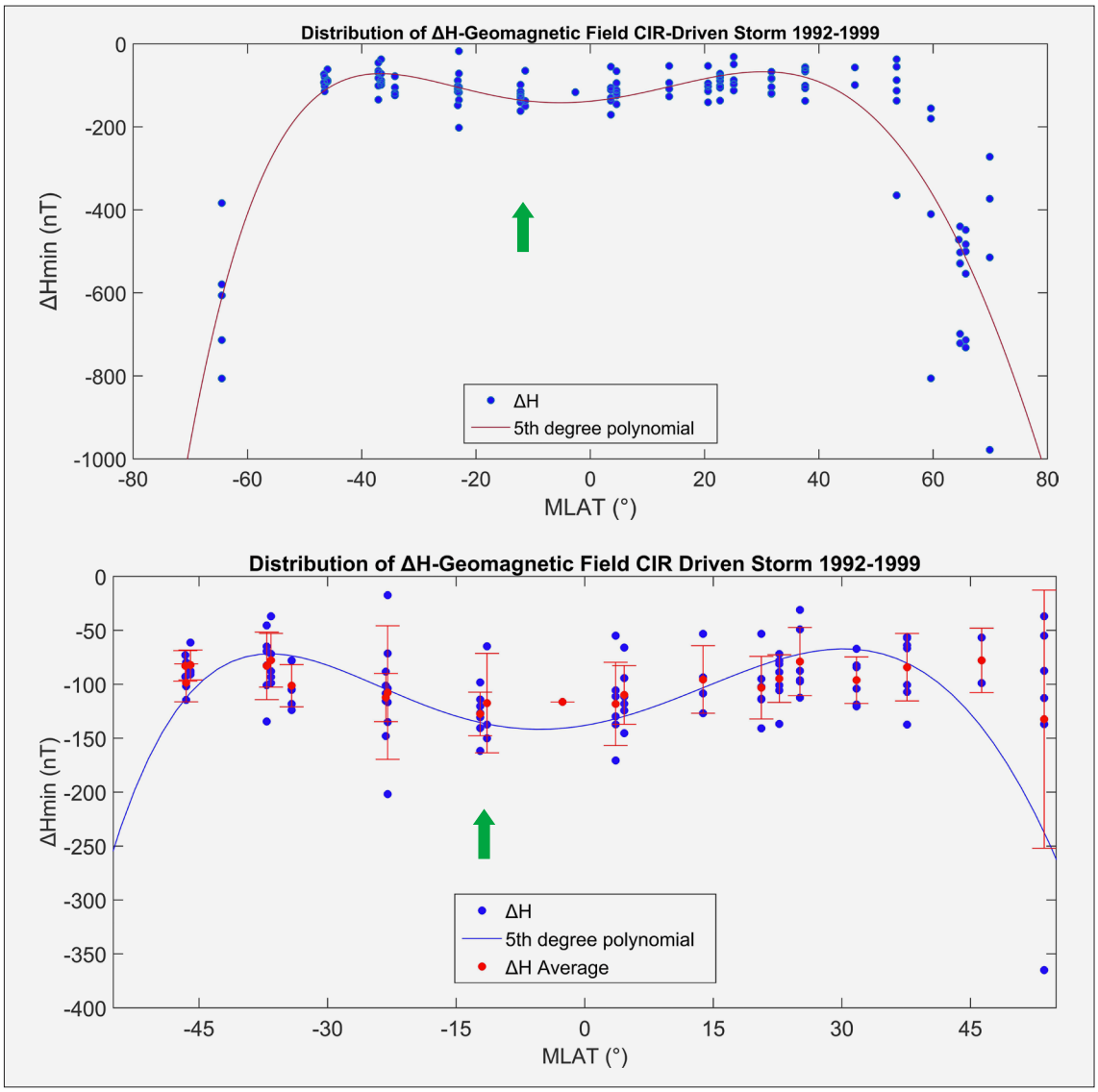


Figure 3: (Top) Latitudinal profile of DH_{min} during CIR-driven storms between 80°N and 80°S; and (Bottom) Average DH_{min} profile during CIR-driven storms between 55°N and 55°S. Note: The green arrows indicate the locations of the Biak and Pontianak observatories.

geomagnetic storms become much more intense as magnetic latitude increases.

The bottom panel of **Figure 2** shows a similar distribution of ΔH_{min} concentrates on a smaller MLAT range, mostly low to mid-latitudes. In contrast to the top figure, the scatter shows that most ΔH_{min} values stay within a reasonable range, often between -100 and −300 nT with fewer extreme outliers. The fluctuation of ΔH_{min} with MLAT is comparatively small and smooth according to the fifth-degree polynomial fit. It is possible that storm-time augmentation of the equatorial ring current or similar current systems is responsible for the modest minimum that is seen close to the magnetic equator. Although the change is not sudden, the graph shows a progressive rise in geomagnetic disturbance approaching mid-latitudes. Here, the latitudinal gradient of ΔH_{min} is weaker than at high latitudes. This suggests that low- and mid-latitude regions react to CME-driven storms more consistently. Deeper negative values that occasionally occur are probably the result of localized or event-specific improvements. The graphic shows that geomagnetic disturbances are less intense and have a smoother spatial structure at lower magnetic latitudes.

Moreover, the distribution of ΔH_{min} during CIR-driven geomagnetic storms across a wide range of magnetic latitudes is depicted in the top panel of **Figure 3**. At high latitudes (|MLAT| > 60°), strongly negative ΔH_{min} values are concentrated, suggesting severe geomagnetic disturbances linked to auroral electrojet activity. ΔH_{min} values are more closely grouped and less negative at low and mid-latitudes, indicating lesser storm-time magnetic field depressions. With slightly constant conditions close to the equator and steep declines toward high latitudes, the 5th-degree polynomial fit clearly shows a latitudinal dependence.

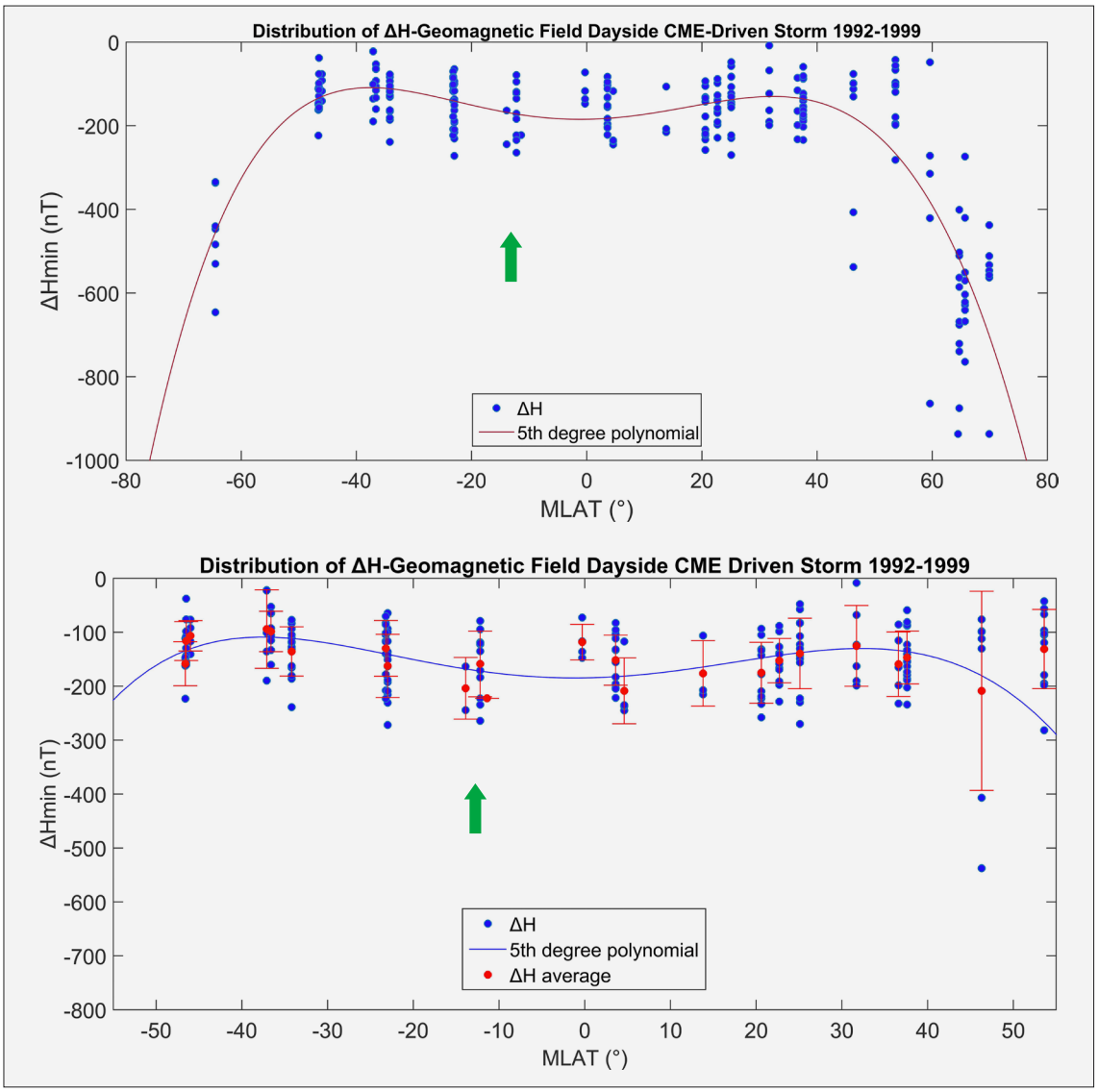


Figure 4: (Top) Latitudinal profile of DH_{min} during dayside CME-driven storms for the period 1992-1999 from 80°N to 80°S, and (Bottom) Latitudinal profile of the average DH_{min} during dayside CME-driven storms from 55°N to 55°S. The green arrows indicate the locations of the Biak and Pontianak observatories.

The low- to mid-latitude response of ΔH_{min} during CIR-driven storms is shown in the bottom panel of **Figure 3**. The majority of data points exhibit slightly similar geomagnetic disturbances with ΔH_{min} range in moderate conditions. The polynomial trend exhibits slightly increased disturbances toward mid-latitudes and a shallow minimum close to the equatorial area. Extreme negative values are typical, indicating little storm impact, in contrast to the high-latitude regions.

The response during CME-driven events shows a more noticeable distinction, drawing on the latitudinal pattern seen for CIR-driven storms. The top panel of **Figure 4** displays the minimal geomagnetic field perturbation (ΔH_{min}) against latitude along the 210° magnetic meridian for dayside CME- and CIR-driven storms. There is a distinct latitudinal pattern that strong negative ΔH_{min} values at high latitudes (|MLAT| > 60°), and indications of a large field depression caused by auroral electrojet activity. Otherwise, the mid- and low-latitude stations observe weaker ΔH_{min} values, usually between -100 and -300 nT that indicating a smaller storm-time influence. Data scattering decreases, and the trend becomes more pronounced when ΔH values are averaged. A fifth-degree polynomial fit for both storm types shows a profile with a large plateau at low to mid latitudes and a sharp decline at high latitudes.

The bottom panel of **Figure 4** shows the ΔH_{min} distribution at low to mid-latitudes is less intense and exhibits greater smoothness compared to the high-latitude data. The polynomial trend shifts gradually across mid-latitudes, indicating steady dayside responses and revealing a slight equatorial minimum that may be associated with the ring or equatorial current systems. Overall, the figure demonstrates that dayside CME-driven storms produce

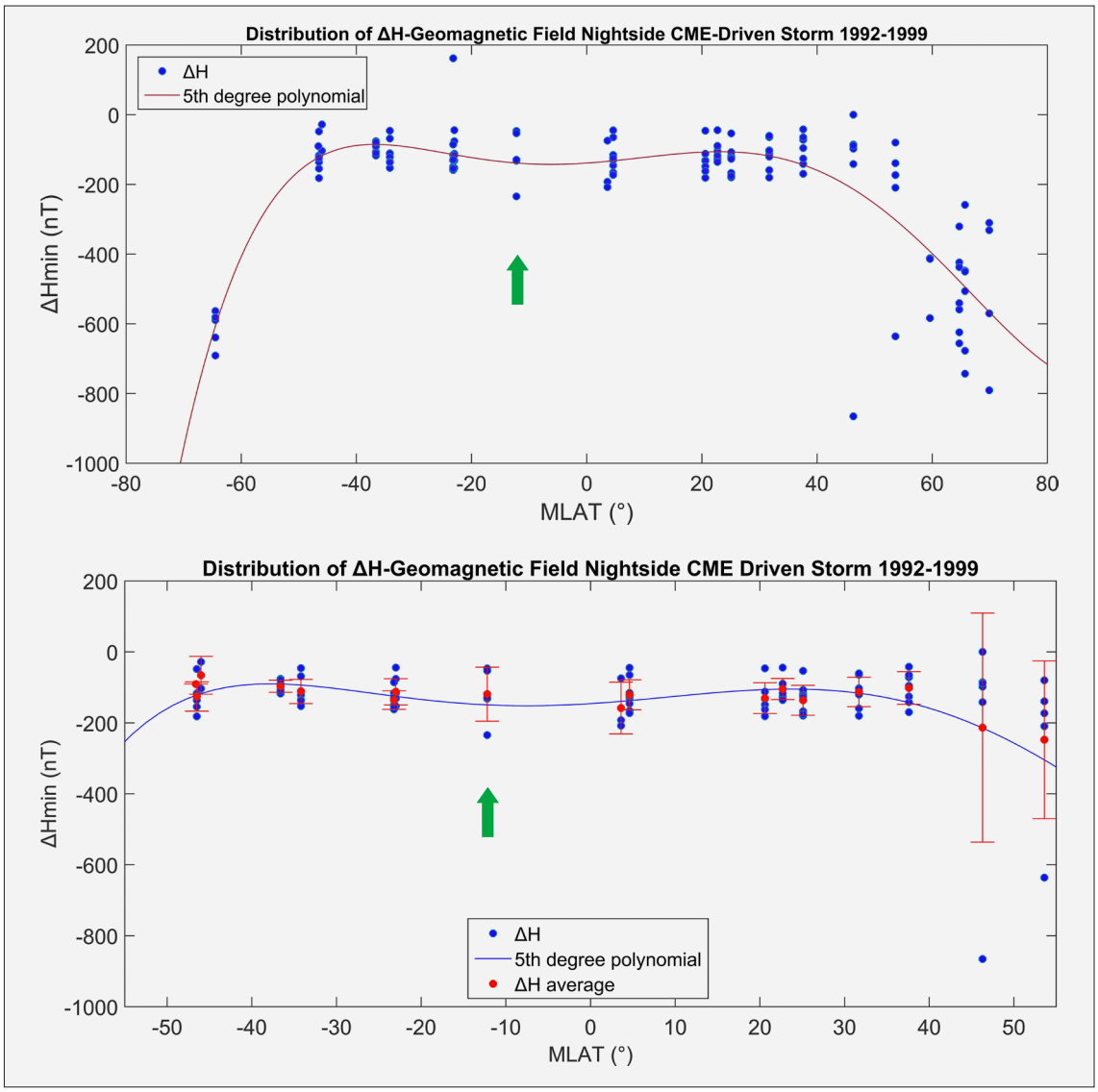


Figure 5: (Top) Latitudinal profile of DH_{min} during nightside CME-driven storms for the period 1992-1999 from 80°N to 80°S; (Bottom) Latitudinal profile of the average DH_{min} during nightside CME-driven storms from 55°N to 55°S. The green arrows indicate the locations of the Biak and Pontianak observatories.

only minor and spatially smooth impacts at lower latitudes, while the most significant geomagnetic disturbances remain confined to high latitudes.

There is an apparent shift in the latitudinal disturbance profile as it crosses from the dayside to the nightside. **Figure 5** presents the latitudinal profile of ΔH_{min} during nightside CME-driven storms, demonstrating the influence of magnetic latitude on geomagnetic field depressions. The top panel indicates that extreme negative ΔH_{min} values are concentrated at high latitudes (more than ±60° MLAT), which reflects strong nightside currents associated with substorms and auroral electrojets. In contrast, low and mid-latitudes show relatively mild disturbances (-100 to -300 nT), suggesting ongoing but reduced storm impacts. Averaging ΔH values reduces data scatter and emphasizes the latitudinal trend.

A direct comparison of the dayside and nightside sectors reveals that ΔH_{min} has a large local-time dependence at high latitudes, which describes its amplitude and structure are generally constant with local time at low latitudes and close to the equator. The Indonesia sector occupies a distinct electrodynamics transition zone during geomagnetic storms, as evidenced by the locations of Biak and Pontianak within the equatorial plateau. As a result, this area directly affects HF communication and GNSS performance in equatorial regions. It also contributes to low-latitude geomagnetically induced currents (GICs) and is strongly associated with ionospheric disturbances in foF2 and TEC.

We now look at these features for a new storm driver after establishing the unique local-time behaviour and specific role of the Indonesian sector. **Figure 6** shows the latitudinal distribution of ΔH_{min} for geomagnetic storms caused by CIRs. The display systematically splits the data into dayside (top panel) and nightside (bottom

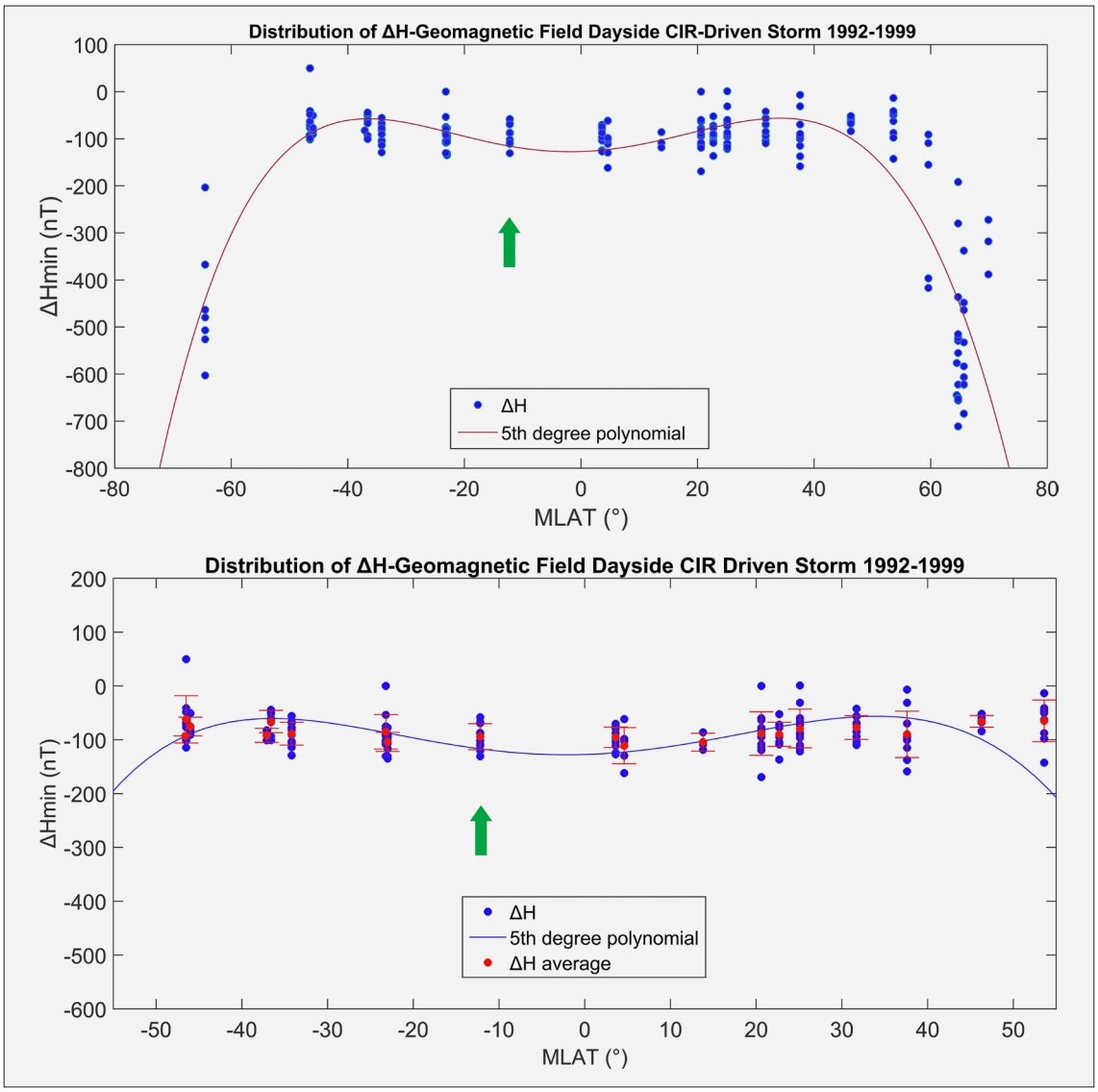


Figure 6: (Top) Latitudinal profile of DH_{min} during the dayside of CIR-driven storms for the period 1992-1999; (Bottom) Latitudinal profile of the average DH_{min} during the dayside of CIR-driven storms between 55°S to 55°N;
Note: The green arrows indicate the locations of the Biak and Pontianak observatories.

panel) sectors and compares broad (±80° MLAT) and narrow (±55° MLAT) latitudinal extents. The main stations at Pontianak and Biak, which correspond to the core equatorial region examined in this study, are indicated by green arrows in **Figure 6**.

Strongly negative ΔH_{min} values are concentrated at |MLAT| > 60° in the top panel, which covers higher latitudes. This suggests that CIR forcing contributes to geomagnetic disturbances linked to auroral electrojet activity. Low- and mid-latitude regions, on the other hand, show more modest ΔH_{min} values, usually between -50 and -200 nT, which indicate weaker dayside geomagnetic impacts. The expected latitudinal trend is apparent and data scatter is decreased when average ΔH values are taken into account. A broad, comparatively flat plateau at low to mid-latitudes is revealed by a fifth-degree polynomial fit to these data, which then sharply declines toward high latitudes. This pattern is consistent with the increasing influence of high-latitude ionospheric currents during CIR-driven storms.

A constant low- to mid-latitude structure is maintained, but a more evident intensification of high-latitude disturbances is revealed when the analysis is focused on the nightside. **Figure 7** shows the latitudinal distribution of ΔH_{min} during nightside CIR-driven geomagnetic storms, demonstrating the contrast between high- and low-latitude responses. Very significant negative ΔH_{min} values are concentrated at |MLAT| > 60° in the top panel, which includes high latitudes. These apparent depressions are indications of strong nightside geomagnetic activity driven by increased auroral electrojets and substorm-related currents. In contrast, the ΔH_{min} values at the low- and mid-latitude regions are significantly milder and are mostly concentrated between −100 and −250 nT. When applied

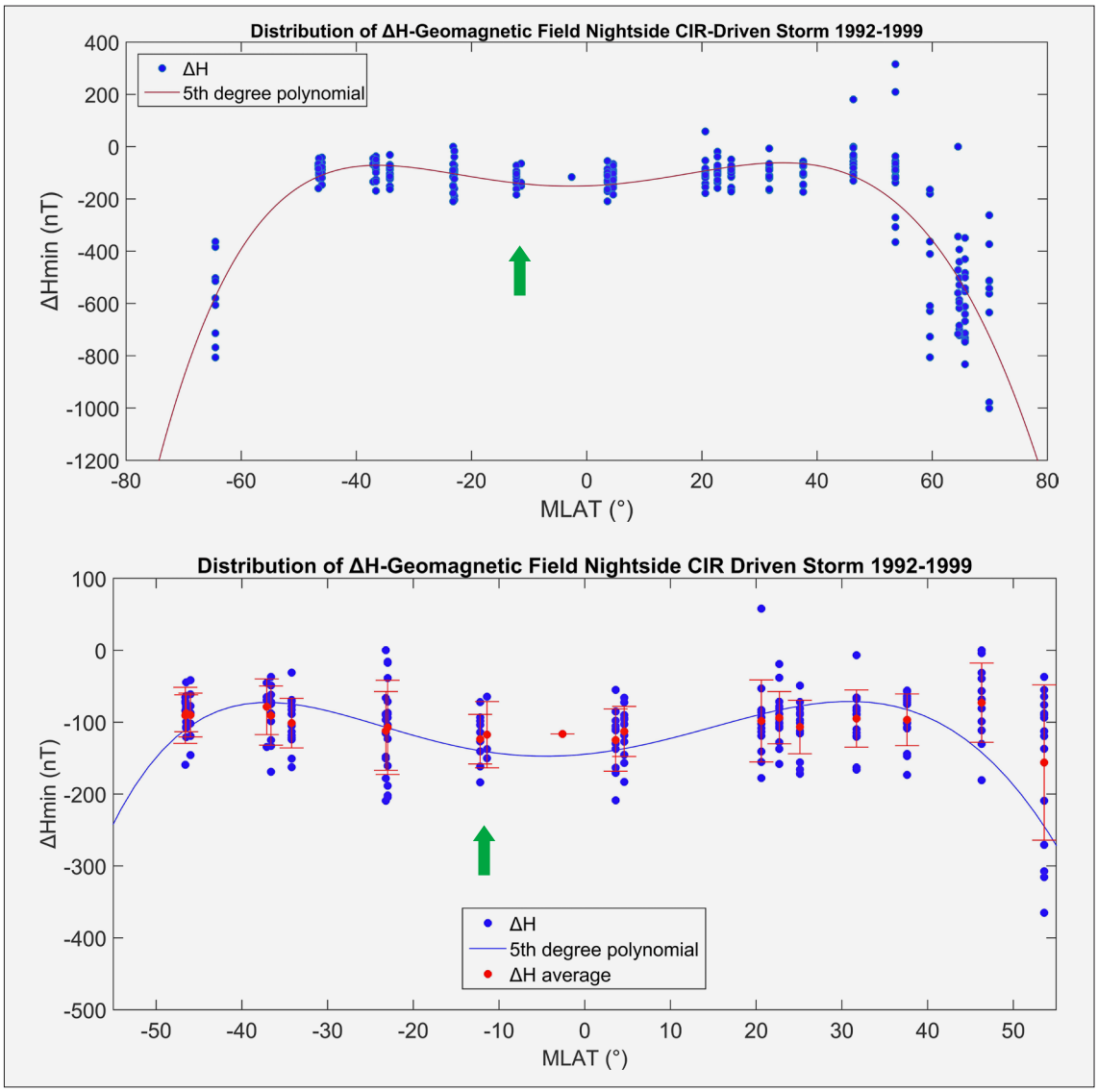


Figure 7: (Top) Latitudinal profile of DH_{min} during the nightside of CIR-driven storms for the period 1992-1999; (Bottom) Latitudinal profile of the average DH_{min} during the nightside of CIR-driven storms between 55°S to 55°N.
Note: The green arrows indicate the locations of the Biak and Pontianak observatories.

to both latitudinal ranges, the fifth-degree polynomial fit reveals a broad, comparatively flat plateau at low to mid-latitudes that changes into a sharp drop toward the poles. The effective deposition of energy in the nightside auroral ionosphere during CIR-driven storms is shown by this sharp gradient. An even smoother ΔH_{min} distribution with less severe outliers can be seen in the bottom panel, which only shows low to mid-latitudes. In this case, the polynomial trend exhibits a shallow minimum close to the equator, suggesting a small contribution from equatorial electrojet systems or ring current. There is broad hemispheric symmetry and little changes within this range.

The normalized latitudinal distribution of the geomagnetic field component (ΔH) for storms caused by CMEs and CIRs is then compared in **Figure 8**. Both storm types produce negative ΔH depressions, which show a decrease in the strength of the horizontal magnetic field during geomagnetic activity, according to the plot. The CME-driven storm profile shows a more apparent and widespread negative excursion compared to the CIR-driven storm profile. Each dataset is fitted with a fifth-order polynomial fit, which smooths observational scatter and reveals the underlying trend. The overall pattern demonstrates that magnetic field depressions are fundamental characteristics of both CME and CIR storm events across all observed latitudes

For all types of storms, the latitudinal profile shows that the largest field depressions are found at higher magnetic latitudes, especially above around 60° MLAT. On the other hand, the low- to mid-latitude region shows a wide and comparatively stable plateau with less severe variations. The polynomial fits show that CME-driven storms produce a steeper gradient and a larger field depression compared to the CIR-driven. In contrast the

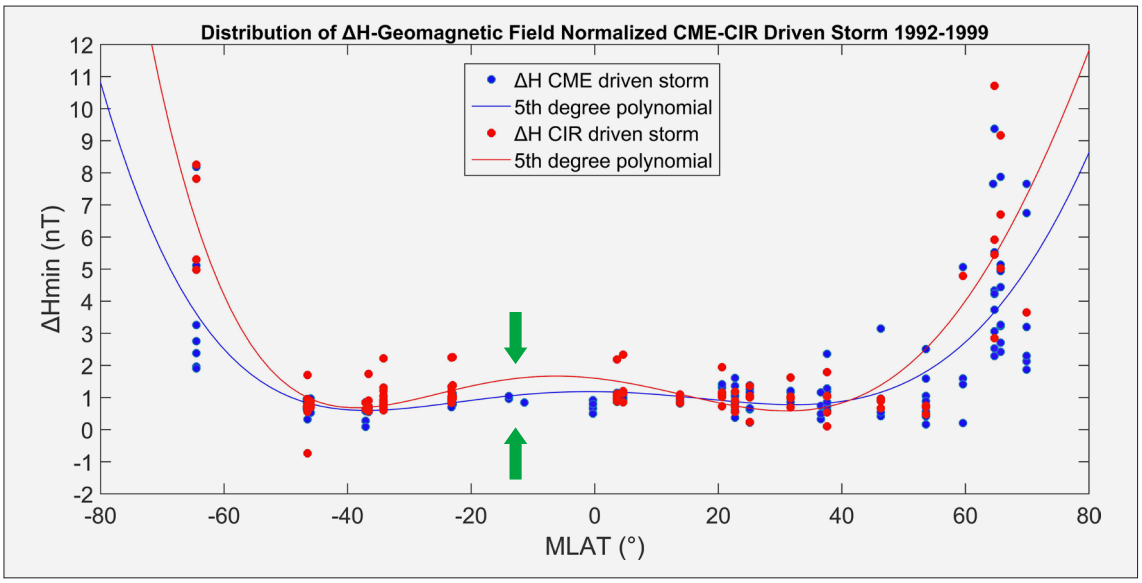


Figure 8: Latitudinal Profile Average of DH_{min} During CME and CIR 1992-1999. The green arrows indicate the locations of the Biak and Pontianak observatories

CIR events are recurring to the more minor disturbances. This comparison emphasizes the stronger and more globally penetrating energy input from CME storms.

Both CME- and CIR-driven storms exhibit a consistent, non-linear inverted omega-shaped (ω) pattern in the latitudinal distributions of ΔH_{min}. Fifth-order polynomial fits reveal the shallow equatorial plateau and more obvious depressions at higher latitudes that characterize this morphology. In conjunction with their higher energy input, a direct comparison reveals that CME-driven storms produce far stronger ΔH_{min} depressions and steeper latitudinal gradients than CIR-driven storms. These features of CME storms are compatible with an atmosphere dominated by prompt penetration electric fields (PPEFs), where magnetospheric electric fields rapidly reach low latitudes. Meanwhile, CIR-driven storms have smaller amplitudes and smoother patterns, which are suggestive of different, less significant coupling mechanisms.

The critical importance of equatorial ionospheric electrodynamics, especially the EEJ, is shown by the substantial equator-centered minimum between about ±5° MLAT. Therefore, these local processes actively shape the low-latitude geomagnetic response rather than it being an inert manifestation of the global ring current. Moreover, the presence of north-south asymmetries, particularly during CME-driven storms, shows that global indices alone are insufficient to explain low-latitude ΔH_{min} variations. Rather, they reflect longitudinally dependent electrodynamics processes involving disturbance dynamo electric fields (DDEFs) during recovery and PPEFs during storm onset.

4. Discussion

Along the 210° magnetic meridian, the latitudinal distributions of ΔH_{min} for storms driven by CMEs and CIRs between 1992 and 1999 show a clearly non-monotonic geomagnetic response (see **Figures 2** and **3**). With its shallow equatorial plateau and prominent high-latitude depressions, the inverted omega (ω)-shaped morphology offers a diagnostic framework for determining the major current systems causing storm-time geomagnetic disturbances. Instead of a continuous decline in the ring current effect with latitude, morphological observations show the simultaneous presence and latitudinal shift of numerous electrodynamics regimes across the equatorial, mid-latitude, and auroral zones.

The storm drivers are directly compared between CME and CIR. It is clear that CME-driven storms result in steeper latitudinal gradients and significantly larger equatorial ΔH_{min} depressions than CIR-driven storms (see **Figure 2 with Figure 3**). The penetration of convective electric fields to low latitudes, a characteristic of PPEFs and impulsive magnetospheric forcing are associated with this behaviour. On the other hand, CIR-driven storms show smoother latitudinal profiles with smaller amplitudes, which are suggestive of gradual and persistent forcing frequently linked to DDEFs. Therefore, it is possible to distinguish between different electrodynamics coupling regimes operating under various solar wind conditions by deliberately separating storm drivers.

A significant decrease of the equatorial ΔH_{min} profile occurs within ±10° MLAT, at the magnetic equator, where the latitudinal gradient is significantly diminished (see **Figures 4** and **5**). This area is equivalent to the equatorial ionospheric electrodynamics domain, where the geomagnetic response is controlled by increased thermal conductivity and equatorial electrojet modulation. ΔH_{min} achieves its weakest depressions at mid-latitudes (±30°–40° MLAT), establishing a transition zone where auroral electrojet influences are minimal and the ring current contributions decrease. Observational limi-

tations on the latitudinal extent and overlap of storm-time current systems are obtained by identifying these gradient transitions.

The observed north-south asymmetries during CME-driven storms, provide proof that symmetric ring current indices cannot account for low-latitude geomagnetic responses (see **Figures 5** and **6**). Instead of purely symmetric magnetospheric current systems, these asymmetries point to the presence of latitude-dependent ionospheric electrodynamics processes, such as PPEFs during storm onset and DDEFs during the recovery phase. Such behaviour is in agreement with other research (**Pulkkinen et al., 2012; Ngwira et al., 2013; Kikuchi & Hashimoto, 2016; Yamazaki and Maute, 2017; Tozzi et al., 2019**) that emphasized the significance of ionospheric electrodynamics for assessing low-latitude storm responses.

This interpretation is further improved by the day-night analysis. Particle injections and substorm-related current systems are associated with CME-driven storms produce the largest ΔH_{min} depressions at high latitudes, with asymmetrical increase and intensified disturbance at mid-to-high latitude during nighttime. In contrast, equatorial ΔH_{min} amplitudes remain unexpectedly constant throughout the day and night. This modest local-time dependence suggests that large-scale electrodynamics forcing is the primary driver of equatorial storm-time responses, rather than local conductivity modulation.

The quasi-steady nature of electrodynamics disturbance produced by prolonged thermospheric heating and wind circulation can be seen in the presence of a broad and narrow equatorial ΔH_{min} plateau that persists on both the dayside and nightside of CIR-driven storms. The equatorial ionosphere is subjected to be lower but longer electrodynamic forcing during CIR-driven events, in contrast to CME-driven storms which produce symmetric and temporally stable low-latitude geomagnetic responses. Similar ΔH_{min} amplitudes observed at Biak, Pontianak, and Yap show that equatorial electrodynamic effects are not confined to the narrow core of the equatorial electrojet region (see **Figure 8**).

The controlled characterization of storm-time geomagnetic morphology across latitude using stations aligned along a single magnetic meridian is a major breakthrough of this study (see **Figure 1**). The observed inverted-omega structure and related gradient transitions can be considered intrinsic latitudinal features instead of artifacts of mixed local-time sampling by limiting longitudinal and magnetic local time variability. A driver-resolved evaluation of equatorial coherence is further made possible by this meridian-based approach, which shows that low-latitude geomagnetic responses are spatially systematic and repeatable across multiple stations. Therefore, under well-constrained longitudinal settings, the results offer an observational baseline for assessing storm-time electrodynamic coupling at low latitudes.

This study demonstrates that the inverted-omega (ω) latitudinal disturbance morphology represents a robust feature of geomagnetic storm responses at low and equatorial latitudes, characterized by a pronounced day-night asymmetry. The results indicate that ionospheric conductivity, thermospheric winds, and storm-time electrodynamic play a dominant role in controlling the observed magnetic variations, with diurnal variability exerting stronger influence than seasonal effects on the morphology. Although the absolute amplitude of ΔH at low latitudes is smaller than at auroral regions, its spatial coherence and intensity remain significant, confirming that the equatorial region is actively involved in storm-time geomagnetic dynamics. The observed geoelectric field magnitudes further suggest that the occurrence of geomagnetically induced currents (GICs) in Indonesia is plausible and potentially significant, even though their magnitudes remain unquantified. It is also emphasized that ΔH and dB/dt, while originating from the same current systems, represent fundamentally different physical quantities and should not be directly interchanged. However, CME-driven storms have bigger ΔH and dB/dt, while, GIC depends on ground conductivity and topology system.

5. Conclusions

Using data from 29 ground-based stations spread along the 210° magnetic meridian (-65° to +70° MLAT), this study used a meridian-constrained, multi-latitude analysis of horizontal geomagnetic field disturbances. The analysis differentiates latitudinal storm-time responses under quasi-constant magnetic local time conditions by examining 91 geomagnetic storms attributed to coronal mass ejections (CMEs) and corotating interaction regions (CIRs) between 1992 and 1999. This enables for a physically consistent comparison across latitude.

For both CME- and CIR-driven storms, a strong inverted omega (ω)-shaped latitudinal morphology of ΔH_{min} appears, suggesting that systematic electrodynamic regimes, rather than storm strength alone, control the large-scale structure of storm-time geomagnetic disturbances. CIR-driven storms show smoother profiles with weaker but more persistent responses, especially at night, reflecting sustained disturbance dynamo processes, whereas CME-driven storms produce much larger ΔH_{min} amplitudes and steeper latitudinal gradients, consistent with impulsive forcing and effective penetration of magnetospheric electric fields. Storm drivers offer a useful framework for resolving dominant coupling mechanisms throughout latitude, as evidenced by the distinct separation of these response patterns.

Low-latitude observations in the Indonesian sector, particularly at BIK and PTN (~11.37°–12.18° S MLAT), reveal DH_{min} amplitudes similar to those observed at other equatorial locations. Rather than being residual expressions of global ring current activity, the spatial co-

herence of these responses demonstrates that equatorial geomagnetic disturbances are systematic and physically significant. These disturbances indicate that low-latitude regions are not magnetically passive during geomagnetic storms and may experience cumulative low-intensity geomagnetically induced currents (GICs), even when the associated magnetic field variations are substantially weaker than those at auroral and subauroral latitudes.

A diagnostic boundary between equatorial and auroral-dominated electrodynamics regimes is additionally established by the finding of a latitudinal transition zone about ±35° to ±50° MLAT. This transition is a significant constraint for GIC vulnerability assessments, which often focus on mid- and high-latitude locations, along with the distinct behaviours of storms caused by CMEs and CIRs. Therefore, it is crucial to include latitudinal electrodynamics structure and storm-driver dependence in GIC risk models, especially for equatorial and low-latitude power systems like those in Indonesia.

This study shows that the inverted-omega (ω) latitudinal disturbance morphology is a robust feature of geomagnetic storm responses at low and equatorial latitudes, exhibiting clear day–night asymmetry controlled by ionospheric conductivity, thermospheric winds, and storm-time electrodynamics, with diurnal variability dominating over seasonal effects. The ΔH amplitudes are smaller than at auroral latitudes, while ΔH and dB/dt of CME-driven storms are bigger than CIR-driven storms. The results emphasize the importance of incorporating low-latitude electrodynamics in geomagnetic storm impact assessments and the need for future quantitative evaluation of GICs in Indonesia.

Data availability statement. Data can be downloaded at the World Data Center for Geomagnetism, Kyoto (https://wdc.kugi.kyoto-u.ac.jp/) and at Plasma and solar wind data center https://omniweb.gsfc.nasa.gov/cgi/nx1.cgi

Acknowledgement

We would like to express our sincere gratitude to Prof. K. Yumoto of Kyoto University and the 210° MM Magnetic Observation Group for generously allowing the use of CPMN geomagnetic data. We also appreciate the World Data Center for Geomagnetism, Kyoto (https://wdc.kugi.kyoto-u.ac.jp/), for providing access to the Dst and IQ day index data and Plasma and solar wind data center (https://omniweb.gsfc.nasa.gov/cgi/nx1.cgi). In addition, we thank all researchers from the Research Center for Space, National Research and Innovation Agency (BRIN), for kindly allowing the use of the Biak and Pontianak geomagnetic data. Their valuable contributions have been essential to this research.

6. References

Ahmad, N., Herdiwijaya, D., Djamaluddin, T., Usui, H., & Miyake, Y. (2018). Diagnosing low earth orbit satellite anomalies using NOAA-15 electron data associated with geomagnetic perturbations. *Earth, Planets and Space*, 70.

DOI:10.1186/s40623-018-0845-5.

Ahmad, N., Kilowasid, L. O. M. M., Fakhrurroja, H., Neflia, Rachman, A., Husin, A., & Fathoni, H. (2025). How geomagnetic storms affect the loss of Starlink satellites in February 2022? *Earth, Planets and Space*, 77.

DOI:10.1186/s40623-025-02154-0.

Barbosa, C. da S., Hartmann, G. A., & Pinheiro, K. J. (2015). Numerical modeling of geomagnetically induced currents in a Brazilian transmission line. *Advances in Space Research*, *55*(4), 1168–1179, doi:10.1016/j.asr.2014.12.008.

Borovsky, J. E., & Denton, M. H. (2006). Differences between CME-driven storms and CIR-driven storms. *Journal of Geophysical Research: Space Physics*, *111*(7), doi:10.1029/2005JA011447.

Boteler, D. H., Pirjola, R. J., & Nevanlinna, H. (1998). The effects of geomagnetic disturbances on electrical systems at the Earth's surface. *Advances in Space Research*, *22*(1), 17–27,10.1016/S0273-1177(97)01096-X.

Burns, A. G., Solomon, S. C., Qian, L., Wang, W., Emery, B. A., Wiltberger, M., & Weimer, D. R. (2012). The effects of Corotating interaction region/High speed stream storms on the thermosphere and ionosphere during the last solar minimum. *Journal of Atmospheric and Solar-Terrestrial Physics*, *83*, 79–87, https://doi.org/10.1016/j.jastp.2012.02.006.

Cane, H. V., & Richardson, I. G. (2003). Interplanetary coronal mass ejections in the near-Earth solar wind during 1996-2002. *Journal of Geophysical Research: Space Physics*, *108*(A4), https://doi.org/10.1029/2002JA009817.

Chapman, S., and Bartels J. (1940). *Geomagnetism.* (Oxford Univ. Press, London, 1940)

Chi, Y., Shen, C., Wang, Y., Xu, M., Ye, P., & Wang, S. (2016). Statistical Study of the Interplanetary Coronal Mass Ejections from 1995 to 2015. *Solar Physics*, *291*(8), 2419–2439, https://doi.org/10.1007/s11207-016-0971-5.

Clúa de Gonzalez A. L., and Gonzalez W. D. (2013). Local-time variations of geomagnetic disturbances during intense geomagnetic storms and possible association with their interplanetary causes, Advances in Space Research, Volume 51, Issue 10, 2013, Pages 1924-1933, ISSN 0273-1177, https://doi.org/10.1016/j.asr.2012.10.029.

Dimmock, A. P., Rosenqvist, L., Welling, D. T., Viljanen, A., Honkonen, I., Boynton, R. J., & Yordanova, E. (2020). On the Regional Variability of dB/dt and Its Significance to GIC. *Space Weather*, *18*(8), https://doi.org/10.1029/2020SW002414.

Fejer, B. G., Jensen, J. W., & Su, S.-Y. (2008). Quiet time equatorial F region vertical plasma drift model derived from ROCSAT-1 observations. *Journal of Geophysical Research: Space Physics*, *113*(A5), https://doi.org/10.1029/2007JA012801.

Hajra, R., & Sunny, J. V. (2022). Corotating Interaction Regions during Solar Cycle 24: A Study on Characteristics and Geoeffectiveness. *Solar Physics*, *297*(3), https://doi.org/10.1007/s11207-022-01953-z.

Kamide, Y., Yokoyama, N., Gonzalez, W., Tsurutani, B. T., Daglis, I. A., Brekke, A., & Masuda, S. (1998). Two-step

development of geomagnetic storms. *Journal of Geophysical Research: Space Physics*, *103*(A4), https://doi.org/10.1029/97JA03337.

Kasran, F. A. M., Jusoh, M. H., Yoshikawa, A., & Mohd. Radzi, Z. (2018). The Time Derivative of the Horizontal Geomagnetic Field for the Low Latitude MAGDAS Langkawi Station for the Estimation of Geomagnetically Induced Current. *Space Science and Communication for Sustainability*, 57–71, doi:10.1007/978-981-10-8011-7_6.

Kataoka, R., & Ngwira, C. (2016). Extreme geomagnetically induced currents. *Progress in Earth and Planetary Science 2016 3:1*, *3*(1), doi:10.1186/s40645-016-0112-x.

Khurshid, M. Z., Aziz, N. F. A., Rhazali, Z. A., & Kadir, M. Z. A. A. (2022). Geomagnetically Induced Current Analysis in Malaysian Power Transmission System. *IEEE Access*, *10*, 110205–110216, doi:10.1109/ACCESS.2022.3214920.

Kikuchi, T., & Hashimoto, K. K. (2016). Transmission of the electric fields to the low latitude ionosphere in the magnetosphere-ionosphere current circuit. *Geoscience Letters*, *3*(1), doi:10.1186/s40562-016-0056-0.

Liu, C.-M., Liu, L.-G., & Yang, Y. (2009). Monitoring and modeling geomagnetically induced currents in power grids of China. *Asia-Pacific Power and Energy Engineering Conference, APPEEC,* doi: 10.1109/APPEEC.2009.4918947.

Love, J. J., & Swidinsky, A. (2014). Time causal operational estimation of electric fields induced in the Earth's lithosphere during magnetic storms. *Geophysical Research Letters*, *41*(7), 2266–2274, doi:10.1002/2014GL059568.

Marshall, R. A., Gorniak, H., Walt, T. Van Der, Waters, C. L., Sciffer, M. D., Miller, M., Dalzell, M., Daly, T., Pouferis, G., Hesse, P., Wilkinson, P. (2013). Observations of geomagnetically induced currents in the Australian power network. *Space Weather*, *11*(1), 6–16, doi:10.1029/2012SW000849.

Ngwira, C. M., Pulkkinen, A., Wilder, V., & Crowley, G. (2013). Extended study of extreme geoelectric field event scenarios for geomagnetically induced current applications. *Space Weather*, *11*(3), 121–131, doi:10.1002/swe.20021.

Pandya, M., Bhaskara, V., Ebihara, Y., Kanekal, S. G., and Baker, D. N. (2019). Variation of radiation belt electron flux during CME- and CIR-driven geomagnetic storms: Van Allen probes observations. *J. Geophys. Res.: Space Phys.*, *124*(8), 6524–6540. https://doi.org/10.1029/2019JA026771.

Pulkkinen, A., Bernabeu, E., Eichner, J., Beggan, C., & Thomson, A. W. P. (2012). Generation of 100-year geomagnetically induced current scenarios. *Space Weather*, *10*(4), doi:10.1029/2011SW000750.

Pulkkinen, A., Bernabeu, E., Thomson, A., Viljanen, A., Pirjola, R., Boteler, D., Eichner , J., Cilliers, P. J., Welling, D., Savani, N., P., Weigel, R., S., Love, J., J., Balch, C., Ngwira, C., M., Crowley, G., Schultz, A., Kataoka, R., Anderson, B., Fugate, D., Simpson, J., J., MacAlester, M. (2017). Geomagnetically induced currents: Science, engineering, and applications readiness. *Space Weather*, *15*(7), 828–856, doi:10.1002/2017SW001622.

Santoso A., Sismanto S., Priyatikanto R., and Martiningrum D. R. (2025a). The intensity of geomagnetic storms associated with the interplanetary magnetic field and solar wind parameters during Solar Cycle 24. *Earth and Planetary Physics 9*: 1–12, 2025 doi:10.26464/EPP2024069

Santoso, A., Sismanto, S., Priyatikanto, R., Hartantyo, E., Mumpuni, E. S., Kilowasid, L. O. M. M., Rachman, A., Nuraeni, F., Filawati, S., Erlansyah, Nurmali, D. (2025b). Assessment of the severe geomagnetic storm on may 10-11, 2024 effects on the geomagnetic field and ionosphere over the indonesian region. *Rudarsko-Geološko-Naftni Zbornik*, *40*(4), 125–136, doi:10.17794/rgn.2025.4.10.

Shen, X.-C., Hudson, M. K., Jaynes, A. N., Shi, Q., Tian, A., Claudepierre, S. G., Qin, M., R., Zong, Q., G., Sun, W.-J. (2017). Statistical study of the storm time radiation belt evolution during Van Allen Probes era: CME- versus CIR-driven storms. *Journal of Geophysical Research: Space Physics*, *122*(8), 8327–8339, doi**:**10.1002/2017JA024100.

Tozzi, R., Coco, I., De Michelis, P., & Giannattasio, F. (2019). Latitudinal dependence of geomagnetically induced currents during geomagnetic storms. *Annals of Geophysics*, *61*(4), doi:10.4401/ag-7977.

Turner, N. E., Mitchell, E. J., Knipp, D. J., & Emery, B. A. (2006). Energetics of magnetic storms driven by corotating interaction regions: A study of geoeffectiveness. *Recurrent Magnetic Storms: Corotating Solar Wind Streams*, 113–124, doi: 10.1029/167GM09.

Uozumi, T., Yumoto, K., Kitamura, K., Abe, S., Kakinami, Y., Shinohara, M., Yoshikawa, A., Kawano, H., Ueno, T., Tokunaga, T., MxNamara, D., Ishituka, J., K., Dutra, S., L., G., Doumbia, V., Obrou, O., Rabiu, A., B., Adimula, I., A., Othman, M., Fairos, M., Otadoy, R., E., S., Otadoy, R. E. S., & MAGDAS Group (2008). A new index to monitor temporal and long-term variations of the equatorial electrojet by MAGDAS/CPMN real-time data: EE-index. *Earth, Planets and Space*, *60*(7), 785–790, doi:10.1186/BF03352835.

Watari, S., Nakamura, S., & Ebihara, Y. (2021). Measurement of geomagnetically induced current (GIC) around Tokyo, Japan. *Earth, Planets and Space 2021 73:1*, *73*(1), doi:10.1186/s40623-021-01448-1.

Yamazaki, Y., & Maute, A. (2017). Sq and EEJ—A Review on the Daily Variation of the Geomagnetic Field Caused by Ionospheric Dynamo Currents. *Space Science Reviews*, *206*(1), 299–405, https://doi.org/10.1007/s11214-016-0282-z.

Yumoto, K., & The 210° MM Magnetic Observation Group. (1996). The STEP 210° Magnetic Meridian Network Project. *Journal of Geomagnetism and Geoelectricity*, *48*, 1297–1309, https://doi.org/10.5636/jgg.48.1297.

Zawawi, A. A., Aziz, N. F. A., Kadir, M. Z. A. A., Hashim, H., & Mohammed, Z. (2020). Evaluation of Geomagnetic Induced Current on 275 kV Power Transformer for a Reliable and Sustainable Power System Operation in Malaysia. *Sustainability, 12, 9225; doi:10.3390/su12219225*.

SAŽETAK

Prema modelu opasnosti od GIC-a za Indoneziju: Analiza latitudinalnih učinaka geomagnetskih oluja na 210. magnetski meridijan

Geomagnetski inducirane struje (GIC) nastaju tijekom geomagnetskih oluja koje mijenjaju ionosferske i magnetosferske strujne sustave od auroralnih do ekvatorskih geografskih širina. Ova studija ispituje latitudinalni odaziv H-komponente (ΔH) tijekom 91 olujnoga događaja (56 uzrokovanih izbacivanjem koronalne mase (CME) i 35 događaja uzrokovanih korotirajućom interakcijskom regijom (CIR)) od 1992. do 1999. godine. Studija se koristi podatcima iz 29 opservatorija duž 210. magnetskoga meridijana (MM), a obje vrste oluja pokazuju izrazitu invertiranu omega (ω) latitudinalnu strukturu, najveću oko aurore, karakteriziranu jakim auroralnim elektromlazom (AE), s minimumima blizu ~±50° magnetske širine i pojačanim poremećajima na niskim geografskim širinama povezanim s ekvatorskim elektromlaznim strujama (EEJ). Oluje uzrokovane CME-om proizvode veće ΔH amplitude i strmije gradijente zbog impulzivnoga djelovanja i električnih polja promptnoga prodiranja (PPEF), dok oluje uzrokovane CIR-om pokazuju slabije, ali trajnije odgovore pod utjecajem procesa poremećaja dinamičkih električnih polja (DDEF). U indonezijskome području, kod Biaka i Pontianaka (~9° – 17° južne magnetske širine), odgovori na niskim geografskim širinama usporedivi su s opažanjima blizu ekvatorskoga područja, što upućuje na učinkovito prodiranje ekvatorske elektrodinamike. Unatoč manjim apsolutnim ΔH amplitudama nego na auroralnim geografskim širinama, ovi odgovori ostaju prostorno koherentni i važni. Prijelazno područje blizu ~±50° magnetske širine i izrazita dnevno-noćna asimetrija između tipova oluja pružaju važna ograničenja za procjenu opasnosti od GIC-a u ekvatorskim energetskim sustavima. Obično je veliki ΔH u olujama uzrokovanim CME-om često popraćen pojačanim dB/dt. Geomagnetske oluje uzrokovane CME-om mogu generirati izražena geoelektrična polja, čak i na niskim geografskim širinama. Rezultati pokazuju da Indonezija nije imuna na opasnosti povezane s GIC-om. Opažena sistematska struktura (ω) i povezana geoelektrična polja pružaju nove spoznaje o potencijalnoj podložnosti indonezijske regije znatnim utjecajima GIC-a, posebno kada su oluje uzrokovane CME-om.

Ključne riječi:
geomagnetska oluja, ekvatorski elektromlaz (EEJ), izbacivanje koronalne mase (CME), korotirajuća interakcijska regija (CIR), 210. magnetski meridijan

Author's contribution

Setyanto Cahyo Pranoto (MD): conceptualization, original draft and writing and formal analysis. **Anwar Santoso** (MD): supervision. **Sismanto Sismanto** (Prof): validation. **Eddy Hartantyo** (Dr): investigation. **Rhorom Priyatikanto** (PhD): methodology. **Nizam Ahmad** (PhD): writing – review & editing. **Kuncoro Wisnu** (MD): project administration. **Mario Batubara** (PhD): ionosphere data visualization. **Silmie Vidiya Fani** (MD): ionosphere data curation. **Siska Filawati** (MD): geomagnetic data curation. **Fitri Nuraeni** (MD): geomagnetic data visualization. **Djohar Syamsi** (MD): software. **Muzirwan** (MD): resources.
All authors have read and agreed to the published version of the manuscript.